Crystal structure and encapsulation dynamics of ice II-structured neon hydrate

Xiaohui Yu[a,b], Jinlong Zhu[a,b,c,d,1], Shiyu Du[e,f,1], Hongwu Xu[g], Sven C. Vogel[b], Jiantao Han[b], Timothy C. Germann[f], Jianzhong Zhang[b], Changqing Jin[a], Joseph S. Francisco[h,i,1], and Yusheng Zhao[a,b,c,d,1]

[a]National Laboratory for Condensed Matter Physics, Institute of Physics, Chinese Academy of Science, Beijing 100190, China; [b]Los Alamos Neutron Science Center Division, [f]Theoretical Division, and [g]Earth and Environmental Sciences Division, Los Alamos National Laboratory, Los Alamos, NM 87545; [e]Division of Functional Materials and Nanodevices, Ningbo Institute of Materials Technology and Engineering, Chinese Academy of Sciences, Ningbo, Zhejiang 315201, China; Departments of [h]Chemistry and [i]Earth and Atmospheric Science, Purdue University, West Lafayette, IN 47906; and [c]High Pressure Science and Engineering Center and [d]Department of Physics and Astronomy, University of Nevada, Las Vegas, NV 89154

Contributed by Joseph S. Francisco, June 9, 2014 (sent for review April 24, 2014)

Neon hydrate was synthesized and studied by in situ neutron diffraction at 480 MPa and temperatures ranging from 260 to 70 K. For the first time to our knowledge, we demonstrate that neon atoms can be enclathrated in water molecules to form ice II-structured hydrates. The guest Ne atoms occupy the centers of D_2O channels and have substantial freedom of movement owing to the lack of direct bonding between guest molecules and host lattices. Molecular dynamics simulation confirms that the resolved structure where Ne dissolved in ice II is thermodynamically stable at 480 MPa and 260 K. The density distributions indicate that the vibration of Ne atoms is mainly in planes perpendicular to D_2O channels, whereas their distributions along the channels are further constrained by interactions between adjacent Ne atoms.

Clathrate hydrates are a group of ice-like, crystalline inclusion compounds formed by water and "guest" gas molecules of suitable size, typically under low-temperature and high-pressure conditions (1). Within a clathrate lattice, water molecules form hydrogen-bonded frameworks and the guest molecules are situated in the framework cavities. Because of this storage capacity, clathrate hydrates have important applications in energy storage and production, gas separation and transportation, and carbon dioxide sequestration.

Depending on the shape and size of the encaged gas molecules, most hydrate clathrates crystallize in one of three distinct crystal structures: cubic sI ($Pm\bar{3}$ n), sII ($Fd\bar{3}$ m), or hexagonal sH ($P6/mmm$) (1). Evidently, the size effect on the crystal structure of clathrate hydrate would be readily expected in systems with the simplest guests, noble gases, which makes research on noble gas hydrate very important for the fundamental thermodynamic understanding of gas hydrates. As expected, large noble gas atoms, such as Ar, Kr, and Xe, form classic clathrates of sI and sII structures at modest gas pressures (i.e., less than 1 GPa) (2–4). However, there was a long-standing controversy about whether smaller noble gas atoms such as He and Ne can form hydrates at all. This issue was not resolved until 1986, when Londono et al. (5) reported the first helium hydrate based on high-pressure neutron diffraction at 280–500 MPa. Unlike traditional clathrate hydrates, He hydrate possesses a filled-ice structure based on that of ice II. Ne is the second-smallest noble gas after He. From differential thermal analysis Dyadin et al. (6) reported indirect evidence of the formation of a classical sII clathrate hydrate between 200–300 MPa. This was later confirmed by Lokshin (7) by neutron diffraction, although no specific structural details were given. When the pressure is further increased to 350 MPa, Lokshin and Zhao (8) found that the sII-structured Ne hydrate breaks down into a pure ice-II structure with no Ne in the framework. Like Ar, the atom size of Ne under this pressure seems to be too large to fit into the free channels in ice-II structure along the c axis.

In this work, we show for the first time to our knowledge, from in situ neutron diffraction experiments that Ne gas can be enclathrated in ice-II channels when the applied gas pressure reaches 480 MPa. To the best of our knowledge, this is the first unambiguous experimental demonstration that Ne hydrate can form an ice II structure. We have also carried out molecular dynamics (MD) simulations of Ne hydrate around 480 MPa to study the distribution of Ne atoms in the host ice-II lattice and to gain insight into mechanisms underlying the hydrate formation. These simulations are of particular importance because, unlike conventional hydrates such as CH_4 or CO_2 clathrates, the ice-II framework of Ne hydrate can be self-stabilized without the encapsulation of guest Ne atoms. This feature is very special in the clathrate hydrate family and thus extends our knowledge of hydrate science.

Results and Discussion

All neutron diffraction patterns were analyzed by the Rietveld method (9) using the General Structure Analysis System (GSAS) (10). A typical refinement example at 480 MPa and 70 K is shown in Fig. 1 after removal of Al diffraction peaks, which originate from the pressure cell. In the entire temperature range studied, Ne hydrate was found to crystallize in space group R-3. A rhombohedral and hexagonal equivalent cell, R-3 H, was used in the refinement, yielding the refined unit cell parameters $a = b \approx 12.9$ Å, $c \approx 6.2$ Å at 480 MPa, 70–260 K. Under these conditions Ne hydrate possesses the same space group as ice II, but with significantly perturbed cell parameters, 0.4% reduction in the c direction, and 0.3% expansion along the a axis at 200 K. The cell parameters measured at different temperatures and 480 MPa are presented in Fig. 2. The thermal expansion coefficients are fitted to $x = x_0 \times \exp \int \alpha(T)dT$, where x = a, c, and V, and $\alpha(T) = \beta + \gamma T$. Over the temperature range of

Significance

Clathrate hydrates have ice-like crystalline structures typically stabled under low-temperature and high-pressure conditions. They are of great importance as potential materials for energy storage and production and carbon dioxide sequestration. Here the first structural refinement data of neon hydrate, to our knowledge, are presented. Both the experimental observations by in situ neutron diffraction and molecular dynamics simulations demonstrate that neon atoms can be enclathrated to form ice II-structured hydrates. The guest Ne atoms occupy the center of ice channels and have substantial freedom of movement owing to the lack of strong bonding between guest molecules and host lattices. The framework of Ne hydrate can be self-stabilized without the encapsulation of guest atoms, which is very special in the hydrate family.

Author contributions: J. Zhu, S.D., J.S.F., and Y.Z. designed research; X.Y., J. Zhu, S.D., H.X., S.C.V., and J.H. performed research; X.Y., J. Zhu, S.D., S.C.V., T.C.G., J. Zhang, C.J., and J.S.F. analyzed data; and X.Y., J. Zhu, S.D., H.X., J. Zhang, and J.S.F. wrote the paper.

The authors declare no conflict of interest.

[1]To whom correspondence may be addressed. Email: jlzhu04@iphy.ac.cn, dushiyu@nimte.ac.cn, francisc@purdue.edu, or Yusheng.Zhao@unlv.edu.

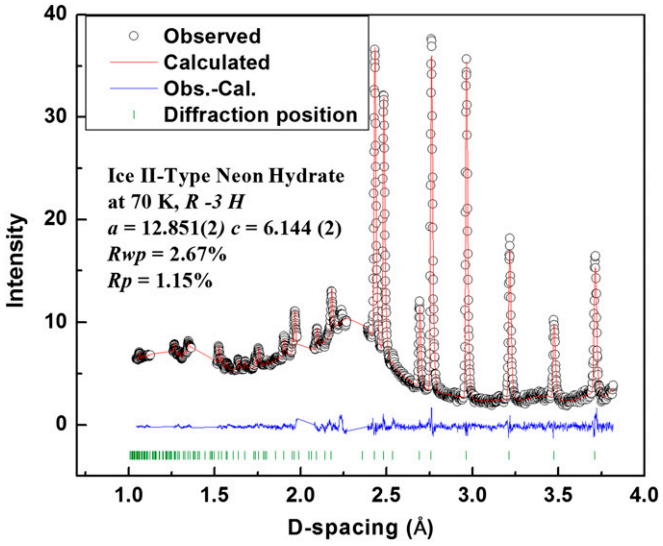

Fig. 1. Rietveld refinement of neutron diffraction data obtained for Ne clathrate hydrate at 480 MPa and 70 K. The observed intensities and calculated pattern are represented, respectively, by circles and a red solid line, and the difference curve is shown below in blue. The tick marks denote the positions of allowed Bragg reflections. All Al peaks from the pressure cell are excluded.

70–260 K, we obtain $V_0 = 898.4$ Å^3, $\beta_v = 1.4 \times 10^{-4}$ K^{-1}, $\gamma_v = 2.8 \times 10^{-7}$ K^{-2}, $a_0 = 6.187$ Å, $\beta_a = 5.1 \times 10^{-5}$ K^{-1}, $\gamma_a = 1.4 \times 10^{-7}$ K^{-2}, $c_0 = 12.95$ Å, $\beta_c = 4.7 \times 10^{-5}$ K^{-1}, and $\gamma_c = 6.8 \times 10^{-8}$ K^{-2}. The cell parameter comparison between Ne hydrate, He hydrate (5), and pure ice II (11) at the same condition (480 MPa, 200K) is also presented in Fig. 2. Although they all have the same D_2O frameworks, the enclosure of He or Ne atoms significantly enlarges the D_2O cages. At 480 MPa and 200 K, for example, the cell volume of Ne hydrate increases by 0.56% compared with that of the pure ice-II structure. As expected, Ne hydrate has a larger cell volume than He hydrate because the atom size of Ne is 19% larger than that of He. Notably, such size and enclosure effects are also reflected in the cell parameter *a*, which follows the same trend as the cell volume (Fig. 2*B*). Strikingly, the variation of the *c* cell parameter (Fig. 2*B*) is in the opposite direction. More detailed discussion on this is presented below.

To shed light on the positions of the Ne atoms in the D_2O cages, diffraction patterns were refined to derive the difference Fourier nuclear density maps (without Ne in the refined models). The difference Fourier map, Fig. 3*A*, clearly indicates the scattering density with the occupied Ne site. It reveals that the incorporated Ne atoms all occupy the center of the D_2O channels. With the help of the difference Fourier map, the atomic positions of Ne hydrate have been refined. Fig. 1 shows a typical refinement for data collected at 480 MPa and 70 K; the corresponding atomic positions are listed in Table 1. Consistent with the difference Fourier map, the Ne atoms are in the center of D_2O cages, with only a slight shift in the *c* direction.

A top view of the refined structure at 480 MPa and 70 K is shown in Fig. 3*B*. The refined atomic positions for Ne are essentially overlapped with the main difference areas revealed by the difference Fourier map (Fig. 3*A*). As expected from the *x* and *y* coordinates in Table 1, $x_{Ne} = y_{Ne} = 0$, the Ne atoms are in the center of the D_2O channels. In Fig. 3*C*, a side view of the Ne hydrate structure, the positions of Ne atoms relative to the D_2O molecules are more clearly illustrated. Unlike the traditional hydrates of sI and sII structures, which need guest gas atoms to stabilize the clathrate frameworks, the ice-II structured Ne hydrate cages/channels can be self-stabilized at 480 MPa. The D_2O cages would not collapse even without any Ne atoms inside. The water molecules form two kinds of hexagonal rings through deuterium bonding in ice-II frameworks, puckered (D1–O1–D2 water molecular) and flat (D3–O2–D4 water molecular), which are also linked by deuterium bonding and D–O bonds (O1–D2–O2). When Ne atoms are incorporated, they are sandwiched by these hexagonal rings.

A comparison of bond lengths and bond angles between pure ice and Ne hydrate is shown in Table 2. Insertion of Ne atoms into the ice structure leads to increases of the deuterium bond distances D1–O1, D3–O2, and D4–O1. This, in turn, results in the lengthening of O1–O1 and O2–O2 distances. The O1–O1 and O2–O2 distances are the distances of oxygen atoms in the two D_2O rings (puckered and flat) in the *a*–*b* plane. The increases of O1–O1 and O2–O2 distances result in the enlargement of the puckered and flat rings because the D_2O molecules are repelled by the Ne atoms through Van der Waals force. This is consistent with the cell parameter increase in the *a*–*b* plane after including Ne atoms. However, the repulsion also decreases the bond angles of O1–D2–O2, which connects the two D_2O rings in the *c* direction. The two D_2O ring are jointly moved in the *c* direction (decrease of O1–O2) by this H-bond, which causes the water cages to shrink in the *c* direction.

We also used MD simulations to investigate the dynamics of Ne atoms in hydrate cages. Ice II-structured Ne hydrate is found to be stable at 260 K and 480 MPa, in good agreement with our observations from neutron diffraction experiments. Fig. 4*A* shows a snapshot of the Ne hydrate structure from a grand canonical Monte Carlo and MD (GCMC+MD) simulation. It is

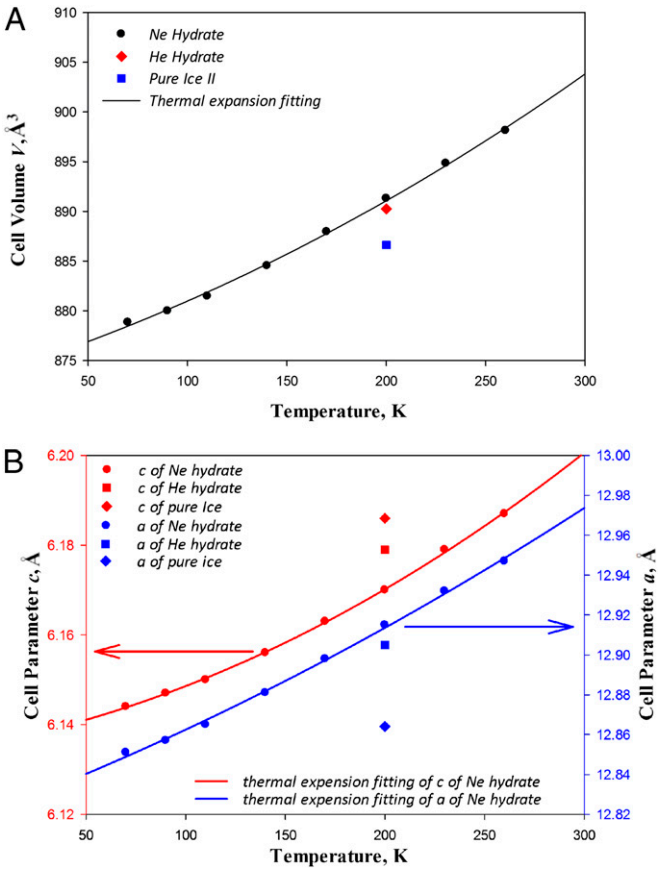

Fig. 2. Temperature dependence of cell parameters of Ne hydrate at 480 MPa (*A*, volume; *B*, lattice parameters *a* and *c*). The data for pure ice II (11) and He hydrate (5) at 480 MPa and 200 K are also presented for comparison.

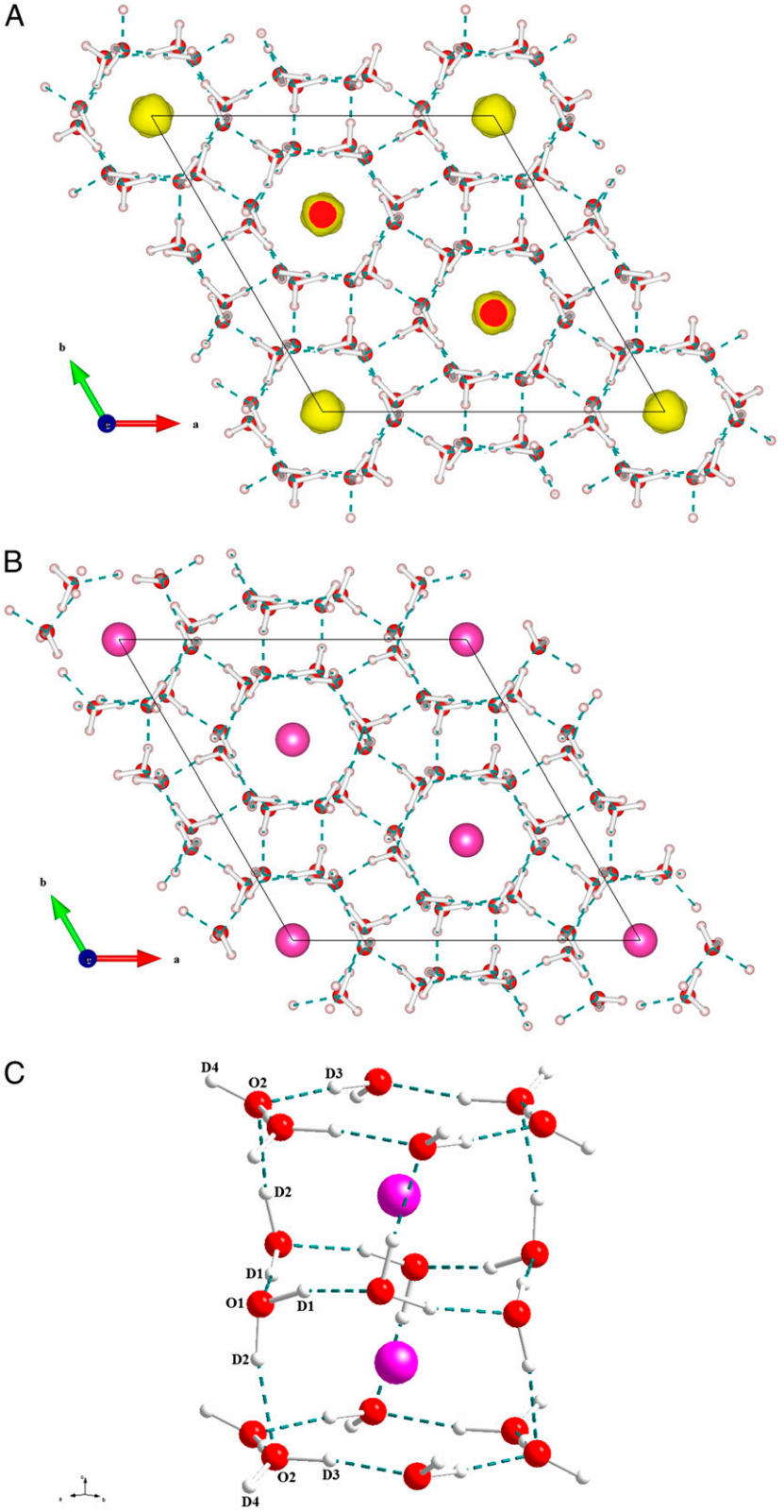

Fig. 3. (*A*) The difference Fourier nuclear density map without Ne atoms in ice cages shows that the incorporated Ne atoms occupy the center of D_2O channels. The isosurface is at 7 fm/Å^3, as shown by the yellow surface. The red dots, which represents higher density of the isosurface, are the intersection of the yellow ball with the cutoff of the unit cell along the (001) plane. The red, white, and purple balls represent O, H, and Ne atoms, respectively (*B* and *C*). The D–O bonds within the D_2O molecule are represented by solid white lines; the hydrogen bonds that connect different D_2O molecules are represented by dashed green lines. (*B*) A top view of the refined crystal structure for Ne hydrate (*c* direction). (*C*) A side view of the refined crystal structure for Ne hydrate. D1–O1–D2 are water molecules in the puckered ring. D1s connect the ring inside and D2s connect the adjacent flat ring. D3–O2–D4 are water molecules in the flat ring. D3s connect the ring inside and D4s connect different channels.

Table 1. Refined fractional coordinates of Ne hydrate at 70 K and 480 MPa with space group *R-3 H* and cell parameters $a = 12.851(2)$ Å and $c = 6.144$ (2) Å

Coordinates	O1	O2	D1	D2	D3	D4	Ne
X	0.2217 (6)	0.1953 (8)	0.1513 (4)	0.2274 (5)	0.1049 (6)	0.2363 (4)	0
Y	0.1955 (7)	0.2340 (5)	0.2060 (5)	0.2186 (5)	0.2113 (6)	0.3083 (7)	0
Z	0.0475 (10)	0.4887 (9)	−0.1480 (8)	0.2074 (7)	0.4873 (10)	0.5582 (8)	0.2608 (20)

Weighted profile R factor = 2.67% and R factor = 1.15%. The U_{ij} of Ne atoms are $U_{11} = 0.0146$, $U_{22} = 0.0146$, $U_{33} = 0.006$, $U_{12} = 0.007$, $U_{13} = 0$, and $U_{23} = 0$. All the numbers in the parentheses are uncertainties for the last significant figures.

notable that there are Ne vacancies in the H_2O cages, which results from the equilibrium between gas and solid phases of Ne in the H_2O cages. At 260 K, Ne occupancy is around 50% from simulation and 31% from the refinement of neutron diffraction data, showing qualitatively good agreement between theoretical predictions and experiments. The difference may be caused by the fact that the simulations are for a single crystal of Ne hydrate, whereas the materials used in the experiments are polycrystalline and may have defects. According to the present MD simulation at 480 MPa and 260K, a significant amount of Ne gas has been dissolved in the cages of the ice sII structure. Meanwhile, Ne atoms are found to be encaged in the lattice by trajectory analysis and the configuration that Ne atoms aggregate to form gas bubbles is not observed, nor is any sign of phase transition for the ice sII lattice. This means that the structure of Ne atoms dissolved in the ice sII structure is thermodynamically stable. We also compared the lattice parameters between the MD simulation and the experiments. At 260 K, we found the lattice parameters for Ne ice II clathrate obtained by MD simulation are $a = 12.92$ Å and $c = 6.20$ Å, which is also very consistent with our structural refinements $a = 12.95$ Å and $c = 6.19$ Å, showing the reliability of our MD simulation. Slightly different from the refinements, in the simulation some Ne atoms are off-centered in the H_2O channel. Although Ne hydrate crystallizes in an ice II-based structure, the Ne atoms still have substantial freedom in the H_2O cages, because there is no direct bonding between the guest Ne and the host H_2O lattices. The temperature-dependent Ne occupancy is shown in Fig. 4*B*. At 70 K, the occupancy of Ne atoms almost reaches 81% based on our refinements. As temperature decreases, the Ne occupancy increases, reflecting a balance between the Ne gas phases and solid phases. The chemical potential of Ne hydrate is described in ref. 12. The Ne atoms in the ice void are in equilibrium with surrounding Ne gas. When the temperature decreases, Ne atoms need to travel from the gas phase to the solid phase (ice cages) to maintain equilibrium, leading to an increasing of Ne occupancy. This temperature-driven occupancy variation of Ne hydrate is similar to that of He hydrate, in which the He occupancy can change with pressure. When pressure increased, the occupancy of He positions was found to increase (5). This is because low temperature or high pressure has a similar effect on the chemical potential equilibrium. However, we also notice that the Ne occupancy can change immediately after the temperature change, as has been observed for H_2 (13). The formation of Ne hydrate is also very fast (within 10 min) when using ice powder as the starting material. For larger gases such as CH_4 and Ar (14, 15), it takes hours to days to form clathrate hydrate from ice powder and guest molecules and the occupancy is not readily changed with temperature. Much more remains to be learned about the limiting mechanisms and kinetics underlying the formation, growth, and dissociation of clathrate hydrate, but as demonstrated by H_2 (13) and our present Ne hydrate results such kinetics have a very close relationship to the guest gas size: For small molecules, the guest gas can more easily travel into or out of the ice vacancies, leading to fast hydrate kinetics.

The thermal vibration of Ne plays a significant role in structural changes of the host framework through D_2O–Ne interactions. Our MD simulation at 260 K and 480 MPa shows that the vibration of Ne atoms is mainly in the (*a*–*b*) planes that are perpendicular to the D_2O channels. Because Ne has an atom size of 2.97Å, the trajectory of Ne atoms can almost fill the entire space of the D_2O cage, as illustrated by the density distribution in Fig. 5*A*. It can be seen that the distribution of Ne along the channel is more restricted in the *c* direction than in the *a*–*b* direction. The global density distribution curves projected on the *a*–*b* (*x*–*y*) and *a*–*c* (*x*–*z*) planes of Ne hydrate are shown in Fig. 5 *B* and *C*, respectively. The spherical symmetry of the Ne projection can be identified in Fig. 5*B*, showing that Ne atoms vibrate within a circular cage in the *a*–*b* plane. From the same figure, no Ne density is found between adjacent channels, indicating that the Ne atoms cannot trespass the boundary between cells along the *a*–*b* plane. Presumably, there is no significant interaction between Ne atoms in different D_2O channels, because the average interatomic distance between adjacent channels can be as long as 7 Å. However, the Ne density distribution along the *c* direction in the *a*–*c* plane (Fig. 5*C*) is nearly continuous, indicating that the Ne atoms have the possibility, although very low, to travel to an adjacent cage in the same channel when it is free of other Ne atoms. However, the average distance between Ne atoms along the *c* direction is only 2.75 Å, so the interaction between Ne atoms in adjacent cages of the same channel cannot be neglected. To demonstrate the relative significance of Ne–Ne interactions in determining the structure of Ne ice II clathrate, we calculated the interaction force between Ne atoms and their surrounding D_2O molecules (Ne–H_2O) and compare it with that between Ne atoms in adjacent cages (Ne–Ne forces). Although diffraction experiments do not provide access to these forces, they can be readily found by MD

Table 2. Comparison of bond lengths and bond angles between pure ice and Ne hydrate

	D1–O1	D3–O2	D2–O2	O1–O1	O2–O2	O1–O2	O2–D2-O1
Pure ice	1.784 (10)	1.787 (7)	1.826 (10)	2.758 (8)	2.744 (6)	2.793 (9)	168.0 (8)
Ne hydate	1.868 (9)	1.788 (8)	1.863 (6)	2.819 (8)	2.751 (6)	2.735 (9)	166.0 (3)

D1–O1 and D3–O2 are the deuterium bonds in two D_2O rings sandwiching Ne atoms; D2–O2 is the deuterium bond connecting the two D_2O rings; O1–O1 and O2–O2 are the bond distances in puckered and flat D_2O rings. O1–O2 stands for the distance of the two rings in the *c* direction; O2–D2–O1 is the bond angle of the deuterium bond and D–O bond that connects the two D_2O rings in the *c* direction. All the numbers in the parentheses are uncertainties for the last significant figures.

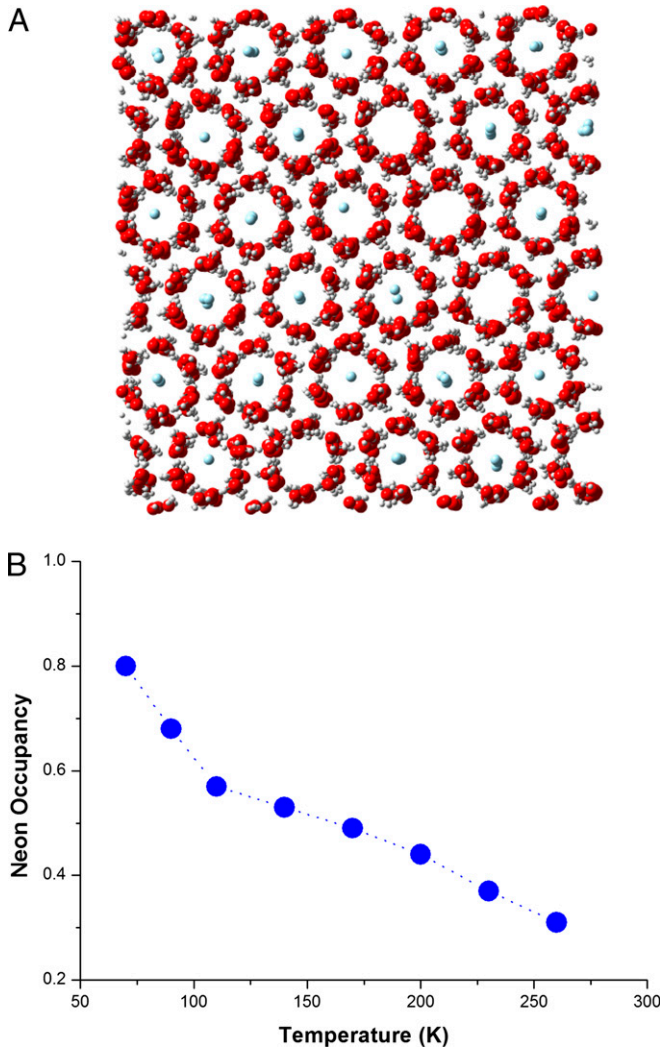

Fig. 4. (*A*) A snapshot of Ne hydrate structure at 480 MPa and 260 K from MD simulation (top view from *c* direction). (*B*) The Ne occupancy change with temperature refined from neutron diffraction patterns.

simulation. The forces on all Ne atoms along the *c* directions are calculated and averaged over all Ne atoms. The repulsive force of (Ne–Ne) is found to be 50% of that of (Ne–H_2O), which means interactions between Ne atoms in adjacent cages have a significant effect in determining the behavior of the clathrate and can play an important role in constraining the Ne atoms in the D_2O cages. This also supports our conclusion that the shortening of the *c* direction in the Ne ice II clathrate structure may also result from Ne–Ne Van der Waals interactions. These interactions can also play an important role in constraining the Ne atoms in the D_2O cages. In addition, the thermal vibration of Ne atoms can be determined by refining the thermal parameter, U_{ij}, in GSAS. Fig. 5*D* shows the temperature dependence of the Ne thermal vibration in the cage. It is clear that our refinement results (Fig. 5*D*) are consistent with the MD simulations (Fig. 5 *A*–*C*). As the result of the D_2O cage configuration and interactions of Ne atoms in the *c* direction, the vibration of Ne atoms in D_2O cages is mainly in the *a*–*b* plane. The interaction between these thermally vibrating Ne atoms and the surrounding H_2O molecules may therefore be responsible for the cage expansion in the *a*–*b* direction. However, in the *c* direction, the Ne atoms are further constrained by other adjacent Ne atoms. The D_2O cages are linked by deuterium bonds, so an expansion in the *a*–*b* direction could cause a shortening in the

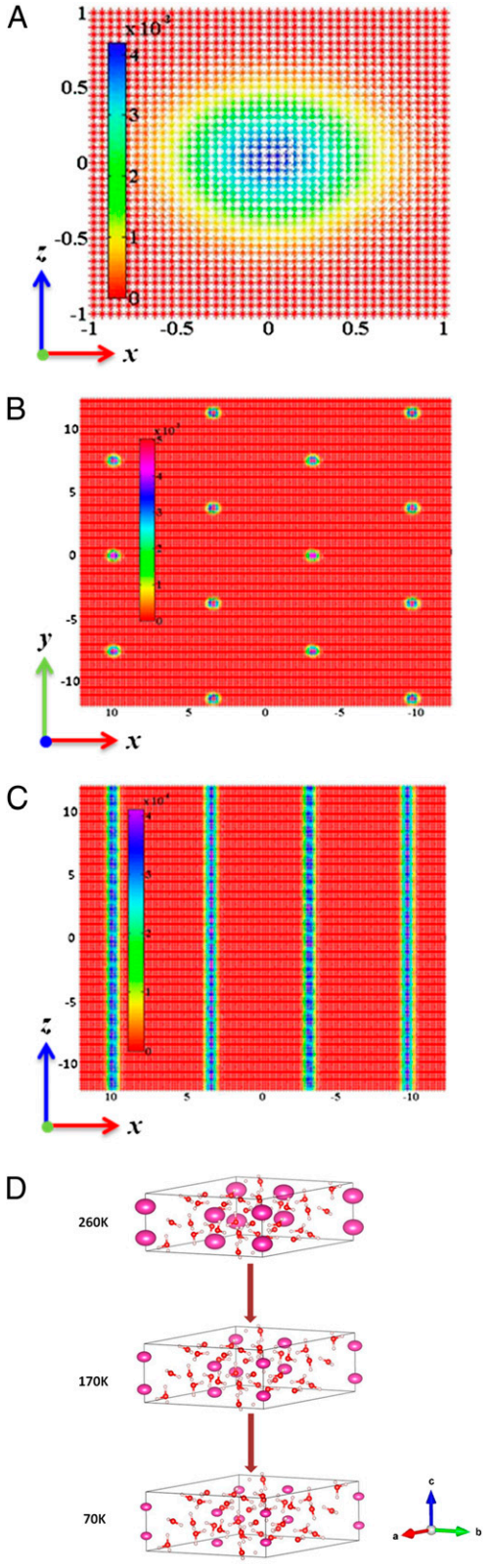

Fig. 5. (*A*) Projection of Ne local density distribution ($\times 10^3$) in a single hydrate cage on the *a*–*c* (*x*–*z*) plane. (*B*) Projection of Ne global density distribution on the *a*–*b* (*x*–*y*) plane. (*C*) Projection of Ne global density distribution on the *a*-*c* (*x*–*z*) plane. The units in *A*, *B*, and *C* are angstroms. (*D*) The vibration of Ne atoms in D_2O cages refined from neutron diffraction patterns at selected temperatures.

c direction. All of these can be reflected by the comparison of bond lengths and bond angles in Table 2. As the temperature decreases, the Ne atoms in D_2O cages become more stable as their thermal vibrations are reduced. This feature is very similar to the classical clathrate hydrate, where the guest molecules are rattling inside the cages.

In conclusion, we present, to our knowledge, the first structural refinement data of Ne hydrate with complete atomic positions and thermal vibration details derived from neutron diffraction experiments. We demonstrate that Ne can form an ice II-structured hydrate at a pressure of 480 MPa, which is stable over a temperature range of 70–260 K. The guest Ne atoms occupy the center of the D_2O channels and are sandwiched by two hexagonal D_2O rings (puckered and flat) through deuterium bonding. MD simulations confirm that the resolved structure for Ne hydrate is thermodynamically more stable than that of pure ice at 480 MPa and 260 K. Dynamically, the Ne atoms have substantial freedom in the D_2O cages owing to the lack of direct bonding between the host and guest molecules. The Ne atoms are instead confined by the Van der Waals interactions with both the D_2O host matrix and the adjacent Ne atoms in the same channels, which lead to the vibration of Ne atoms mainly in the *a*–*b* plane. As the temperature decreases, the occupancy of Ne in the cage increases rapidly to fulfill the gas–solid equilibrium required by the chemical potential. The vibration of Ne plays an important role in affecting the D_2O cage structures.

Materials and Methods

The sample synthesis and time-of-flight neutron diffraction studies of Ne hydrate were performed under high-pressure/low-temperature conditions at the Los Alamos Neutron Science Center (LANSCE), Los Alamos National Laboratory. Neutron diffraction is chosen because the title material is composed of elements that are light and thus have weak X-ray scatters. Furthermore, neutrons can penetrate the required aluminum gas pressure cells. We used an experimental setup specifically designed for the high-pressure preferred orientation (16) diffractometer at the pulsed spallation neutron source LANSCE. The setup consists of a cylindrical aluminum gas cell, allowing working pressures up to 600 MPa. To minimize the background from incoherent scattering of hydrogen, 99.8% deuterated ice, D_2O, was used as the starting material. The Ne gas (99.9% purity) was purchased from Airgas Inc.

To accelerate the synthesis kinetics, deuterated ice was first crushed to fine powder in a coffee grinder at the refrigerator temperature of 240 K and was then loaded into a precooled Al gas-pressure cell. The cell was sealed and attached to the tip of a displex cold finger, followed by the evacuation and recycling of Ne gas five times to expel room air from the entire gas-line system. Neutron diffraction data were collected at an applied Ne gas pressure of 480 MPa and temperatures from 260 to 70 K. To obtain sufficient statistics for reliable structure refinement, all data were collected for an integration time equivalent to 1 h at a current of 100 μA, thus compensating for potential beam fluctuations during the data collection. Because no substantial preferred orientation was present, data of the 8 140° and 10 90° detector panels were integrated, yielding two histograms that were analyzed simultaneously using the GSAS package. The GSAS peak profile function 1 was used to describe the measured diffraction peaks. The thermal motion of O and D atoms was assumed to be isotropic; only Ne atoms are refined as anisotropic because they are confined in the D_2O cages by Van der Waals force.

The combination of in situ experiment with MD simulations provides both a benchmark for the experimental data as well as further insight into structural evolution and formation mechanisms, especially for the clathrate hydrate studies (17, 18). In this work, the MD simulations were also performed to study the stability of Ne hydrate and the dynamics of Ne guest atoms in the host framework. Simulations were conducted at 480 MPa and 260 K in an isothermal–isobaric (NPT) ensemble enforced via a Nosé–Hoover (19, 20) thermostat and barostat. The TIP4P water model (21) was adopted to calculate the interaction between H_2O molecules. The interactions between H_2O molecules and Ne atoms are modeled with a Lennard–Jones (LJ) potential. The Ne–Ne LJ parameters are $\sigma = 2.755$ Å and $\varepsilon = 0.0826$ kcal/mol (12), and those between Ne atoms and H_2O molecules are $\sigma = 3.12$ Å and $\varepsilon = 0.116$ kcal/mol, where the van der Waals centers for H_2O are on O atoms. The charge on the Ne atoms is zero and the long-range electronic interactions between H and O atoms are computed with the particle–particle particle–mesh method (22). The dimension of the periodic simulation box is $38 \times 37 \times 37$ Å^3, which is constructed by duplication of unit cells of an Ne hydrate cage. The total simulation time is 4.5 ns using a time step of 1.0 fs. The spatial distribution of Ne atoms in the hydrate cage is estimated with MD trajectories. We also performed a hybrid GCMC+MD simulation to examine the equilibrium Ne concentration in hydrate cages determined by chemical potential equilibrium, in which 3×10^6 steps are carried out. The simulations were performed with the LAMMPS software package (23).

ACKNOWLEDGMENTS. This work has benefited from the use of the Lujan Neutron Scattering Center at Los Alamos Neutron Science Center, which is funded by the Department of Energy's Office of Basic Energy Sciences. This research was supported by Los Alamos National Laboratory, which is operated by Los Alamos National Security LLC under Department of Energy (DOE) Contract DEAC52-06NA25396. The work at Institute of Physics, Chinese Academy of Sciences was funded by the Chinese Academy of Sciences project under Contracts KJCX2-YW-W26 and XDB07000000. This research was sponsored in part by the National Nuclear Security Administration under the Stewardship Science Academic Alliances program through Department of Energy Cooperative Agreement DE-NA0001982.

1. Sloan ED, Jr (1998) *Clathrate Hydrates of Natural Gases* (Dekker, New York), 2nd Ed.
2. Itohaand H, Tse JS, Kawamura K (2001) The structure and dynamics of doubly occupied Ar hydrate. *J Chem Phys* 115(20):9414–9420.
3. Tse JS, et al. (2005) Anharmonic motions of Kr in the clathrate hydrate. *Nat Mater* 4(12):917–921.
4. Sanloup C, Mao Hk HK, Hemley RJ (2002) High-pressure transformations in xenon hydrates. *Proc Natl Acad Sci USA* 99(1):25–28.
5. Londono D, Kuhs V, Finney JL (1988) Enclathration of helium in ice II: The first helium hydrate. *Nature* 332:141–142.
6. Dyadin YA, et al. (1999) Clathrate hydrates of hydrogen and neon. *Mendeleev Commun* 9(5):209–210.
7. Lokshin KA (2005) Multiple cage occupancy and crystal structure variations in natural gas clathrate hydrates. *Proceedings of the Fifth International Conference on Gas Hydrates 2005* (Tapir Academic, Trondheim, Norway), pp 427–430.
8. Lokshin KA, Zhao Y (2005) Advanced setup for high-pressure and low-temperature neutron diffraction at hydrostatic conditions. *Rev Sci Instrum* 76(6):063909.
9. Rietveld HM (1969) A profile refinement method for nuclear and magnetic structures. *J Appl Cryst* 2(2):65–71.
10. Larson AC, Von Dreele RB (1990) *General Structure Analysis System (GSAS)* (Los Alamos National Laboratory, Los Alamos, NM), Los Alamos National Laboratory Report LAUR 86-748.
11. Lobban C, Finney JL (2002) The *p*–*T* dependency of the ice II crystal structure and the effect of helium inclusion. *J Chem Phys* 117(8):3928–3934.
12. Hakim L, Koga K, Tanaka H (2010) Novel neon-hydrate of cubic ice structure. *Physica A* 389(9):1834–1838.
13. Lokshin KA, et al. (2004) Structure and dynamics of hydrogen molecules in the novel clathrate hydrate by high pressure neutron diffraction. *Phys Rev Lett* 93(12):125503.
14. Stern LA, Hirby SH (1998) Polycrystalline methane hydrate: Synthesis from superheated ice and low-temperature mechanical properties. *Energy Fuels* 12(2): 201–211.
15. Davidson DW, Handa YP, Ratcliffe CI, Tse JS (1984) The ability of small molecules to form clathrate hydrate of structure II. *Nature* 311:142–143.
16. Wenk HR, Lutterotti L, Vogel CS (2003) Texture analysis with the new HIPPO TOF diffractometer. *Nucl Instrum Meth A* 515(3):575–588.
17. Kuhs WF, Chazallon B, Radaelli PG, Pauer F (1997) Cage occupancy and compressibility of deaterated N_2-clathrate hydrate by neutron diffraction. *J Inclus Phenom Mol* 29(1): 65–77.
18. Mulder FM, Wagemaker M, van Eijck L, Kearley GJ (2008) Hydrogen in porous tetrahydrofuran clathrate hydrate. *ChemPhysChem* 9(9):1331–1337.
19. Evans DJ, Holian BL (1985) The Nose-Hoover thermostat. *J Chem Phys* 83(8): 4069–4074.
20. Martyna GJ, Klein ML, Tuckerman M (1992) Nosé–Hoover chains: The canonical ensemble via continuous dynamics. *J Chem Phys* 97(4):2635–2643.
21. Horn HW, et al. (2004) Development of an improved four-site water model for biomolecular simulations: TIP4P-Ew. *J Chem Phys* 120(20):9665–9678.
22. Sadus RJ (1999) Particle-particle and particle-mesh (PPPM) methods. *Molecular Simulation of Fluids* (Elsevier Science, Amsterdam), pp 162–169.
23. Plimpton S (1995) Fast parallel algorithms for short-range molecular dynamics. *J Comput Phys* 117(1):1–19.